Kainate receptors are critical for permissivity to sustained, disorganized and network-wide pathological activity in the epileptic Dentate Gyrus

Lucas Goirand-Lopez[1], Pascal Benquet[2], Mariam Alharrach[2], Bruno Delord[3]#*, Valérie Crépel[1]#*

1. INMED, INSERM, Aix-Marseille University, France
2. University of Rennes, Inserm-U1099, LTSI, Rennes, France
3. Institut des Systèmes Intelligents et de Robotique (ISIR), Sorbonne University, CNRS, Paris, France.

# These authors contributed equally: Valérie Crépel, Bruno Delord

* Corresponding authors. E-mail addresses: valerie.crepel@inserm.fr - bruno.delord@sorbonne-universite.fr

Abstract

In temporal lobe epilepsy, the dentate gyrus (DG) undergoes extensive reorganization through recurrent mossy fiber (rMF) sprouting, engaging both AMPA and kainate receptors (KARs) at granule cell–granule cell (GC–GC) synapses. While KARs are known to enhance neuronal excitability, their specific contribution to epileptogenic rMF network dynamics remains poorly understood. Here, building and assessing a DG network model endowed with KARs, we revealed that slow KAR-EPSPs – which synergistically interacted with persistent sodium currents – profoundly reshaped epileptogenic dynamics by lowering the threshold for pathological activity, through two complementary mechanisms. Regarding structural constraints on the network, KARs reduced the number of sprouted connections required to drive epileptiform discharges. Concerning functional constraints on DG inputs, KARs extended the window for temporal integration, increased network responsiveness, enabling aberrant activities in response to more dispersed input patterns. Actually, the extension of the structural and functional parameter region driving epileptiform activity was effective both for their initiation and, critically, their sustained maintenance. Moreover, KARs drove a striking transition in network behavior, from partially organized collective dynamics to a highly disordered regime. Notably, in the presence of KARs, firing massively invaded the DG network, disorganizing spiking patterns, which resulted in increased dimensionality and entropy of activity, and a drop of mutual information between neurons. Altogether, our results suggest that KARs are not merely amplifiers of network excitation but rather represent consubstantial determinants that fundamentally alter the dynamical landscape, rendering sprouted dentate gyrus network permissive to self-sustaining pathological activity.

Introduction

Temporal lobe epilepsy (TLE) is recognized as the most common form of epilepsy in adults (Helmstaedter et al., 2025; Téllez-Zenteno and Hernández-Ronquillo, 2012). It is characterized by substantial pathological changes in the hippocampus, particularly through mechanisms of reactive plasticity (Téllez-Zenteno and Hernández-Ronquillo, 2012). This plasticity is prominently observed in the dentate gyrus, where surviving neurons form aberrant connections, leading to significant network reorganization (Buckmaster, 2012; Gabriel, 2004; Represa et al., 1989; Sutula et al., 1989). A critical feature of this reorganization is the pathological sprouting of recurrent mossy fibers (rMFs), which establish aberrant excitatory synapses between dentate granule cells (GCs : GC-GC synapses). Previous studies have demonstrated that synaptic transmission within this aberrant recurrent network is mediated by both AMPA receptors (AMPARs) and kainate receptors (KARs) (Artinian et al., 2015, 2011; Epsztein et al., 2005).

Among KARs, GluK2-containing subunits have been identified as critical in enhancing network excitability and facilitating seizure activity (Peret et al., 2014). Preclinical studies have underscored the therapeutic potential of targeting KARs, demonstrating that their blockade significantly reduces seizure frequency in TLE mouse models and suppresses epileptiform discharges in organotypic hippocampal slice cultures prepared from surgically resected tissue of drug-resistant TLE patients (Baudouin et al., 2024; Boileau et al., 2023; Peret et al., 2014). Recent observations using single-cell-resolution calcium imaging have further elucidated the role of KARs in promoting epileptic network activity, particularly by recruiting neurons into large coactive assemblies (Goirand-Lopez et al., 2023).

Despite these findings, a critical question remains: how does the interplay between the degree of sprouted GC-GC connectivity and the contribution of KARs at these synapses determine the threshold and the dynamics of epileptiform activity? Experimentally probing this structural-functional interplay poses significant challenges, as experimental tools to independently manipulate both the density of GC-GC synapses and their AMPAR/KAR composition in animal models are currently limited. To address these complexities, we adapted the Santhakumar computational model of the dentate gyrus, which provides a detailed simulation of this brain region (Morgan et al., 2007; Santhakumar et al., 2005). The

Santhakumar model is a representation of the dentate gyrus that consists of a reduced network of 527 cells, including 500 granule cells, 15 mossy cells, 6 basket cells, and 6 HIPP cells, reflecting the cellular proportions of the biological dentate gyrus. Each cell is modelled with an intricate multi-compartment architecture that includes both somatic and dendritic elements. The initial network structure includes AMPAR-mediated excitatory and GABAergic inhibitory synapses arranged in a biologically realistic ring topology that reflects the natural lamellar organization and the GC-GC connectivity. This framework enables a systematic exploration of how different levels of GC-GC synapses (ranging from 0% to 50%) affect pathological network dynamics. However, the original model did not account for KAR-mediated transmission at GC-GC synapses, an essential aspect of the epileptic network. In the present study, we extended this model by incorporating KAR-mediated synaptic responses at GC-GC synapses and their amplification by INaP, consistent with experimental observations (Artinian et al., 2011; Baudouin et al., 2024; Boileau et al., 2023; Epsztein et al., 2010, 2005; Matsuda et al., 2016; Peret et al., 2014). Our findings show that KAR-mediated transmission at GC–GC synapses acts as a critical driver of dentate gyrus epileptiform activity by lowering both structural and functional activation thresholds. In doing so, KARs transform transient, locally confined responses into sustained, network-wide reverberating activity, characterized by high-dimensional, disorganized population dynamics. Together, these effects reveal that KARs represent key orchestrators in the impairment of normal dentate gyrus "gating" (Hsu, 2007), by rendering the sprouted network vulnerable, due to its increased permissivity to self-sustaining persistent pathological activity.

Results

Our work aimed to link synaptic transmission to network dynamics to explain how KAR-mediated signaling shapes DG epileptiform activity in TLE, building on the Santhakumar computational model (Morgan et al., 2007; Santhakumar et al., 2005). First, we developed and validated a GC-GC synapse model integrating AMPAR- and KAR-mediated EPSP kinetics with INaP, constrained by experimental patch-clamp recordings, to capture EPSP amplitude, dynamics, and voltage-dependent amplification (Artinian et al., 2015, 2011; Epsztein et al., 2010). Next, we assessed how receptor composition governs temporal integration at GC–GC synapses and quantified its impact on GC spiking. Finally, we embedded these mechanisms in a biophysically detailed DG network to test how KAR inclusion at GC-GC synapses modulates both the threshold for DG excitability and the spatiotemporal landscape of epileptiform activity.

A novel biophysical model with kainate receptors at sprouted GC–GC synapses

First, we developed a biophysical model of GC-GC synapses that incorporated both AMPARs and KARs, which had distinct conductances. The model parameters were derived from experimental data from patch-clamp recordings (Epsztein et al., 2010). The model incorporated two key features of KARs relative to AMPARs: slower conductance deactivation kinetics and a lower maximal conductance, consistent with previous experimental observations. Postsynaptic response amplitudes were scaled appropriately to match experimental excitatory postsynaptic potentials (EPSPs) (Artinian et al., 2011). We incorporated the persistent sodium current (INaP), to account for the voltage-dependent amplification of EPSPs in these synapses, using steady-state activation from a previous modeling study (Lee, 2007), with parameters adjusted to fit our experimental data (see Methods). Among them, the time constant of activation was fitted using a simplified model (see Methods) to account for the amplification of EPSPs by INaP at subthreshold membrane potentials (Vsubthreshold) relative to those at resting membrane potential (Vrest). The quality of that fitting procedure was confirmed by comparing EPSPs in the complete neuronal model (see Methods) with experimental recordings. Both modelled AMPAR-(black) and KAR-(red) EPSPs (Fig. 1A1, 1B1) closely matched experimentally recorded EPSPs (Fig. 1A2, 1B2), both when synaptic current waveforms were injected (Fig. 1A1, 1A2), or synaptically

triggered by electrical stimulation (Fig. 1B1, 1B2). In particular, both KAR-mediated EPSPs' larger amplification at subthreshold potentials as well as their slower decay, compared to AMPAR-mediated EPSPs, were clearly reproduced in the model. Therefore, the model captured key features – amplitude, dynamics, and voltage-dependent properties – of both AMPAR- and KAR-EPSPs (Epsztein et al., 2010), validating the parameter choices.

We next assessed whether the model could account for the temporal integration of AMPAR- and KAR-EPSPs and their impact on GC spiking, as observed experimentally (Artinian et al., 2011). Regarding temporal integration (Fig. 2A1, 2A2), KAR-EPSPs (Fig. 2A1, red) exhibited more pronounced summation in response to trains of synaptic stimulation at subthreshold membrane potentials, compared to AMPAR-EPSPs (Fig. 2A1, black), as found experimentally (Fig. 2A2) (Artinian et al., 2011). The model accounted for this effect across all conditions tested experimentally, i.e., at resting potential and subthreshold potentials, both with and without the INaP. Notably, the model reproduced the synergistic interaction between KARs and INaP, which significantly amplified EPSP summation at subthreshold potentials (Artinian et al., 2011).

We then examined the impact of the temporal integration of AMPAR- and KAR-EPSPs on GC spiking. EPSP trains produced more spikes in the presence of KARs than in the presence of AMPARs (Fig. 2B1, 2B2), resulting in an input-output frequency relationship with a steeper slope (Fig. 2C1, 2C2), consistent with experimental data (Artinian et al., 2011).

Overall, the model thus accurately reproduced key effects of KARs, i.e., EPSPs with slower dynamics and synergistic amplification by INaP at subthreshold potentials, which, in turn, allowed greater temporal integration and higher output firing rates than those produced by AMPARs.

KARs at sprouted GC–GC synapses extend the temporal integration and increase spike probability

We then leveraged from previous cellular-level steps, which allowed to design an experimental data-fitted GC model, to further explore the impact of AMPARs and KARs at

the level of network interactions, to form specific predictions on the effects of these synaptic currents on collective DG network dynamics at the global scale of the epileptic DG.

To investigate this, we first evaluated how these effects are expressed in the sprouted GC-GC network, by evaluating the response of GCs in terms of spiking probability, as a function of the window duration of GC inputs and of the in-degree of a GC-GC network architecture in which multiple presynaptic GC inputs converged onto a single postsynaptic GC (Fig. 3). For this analysis, we either considered only AMPAR (*100%AMPAR* condition) or 50% AMPAR and 50% KAR (*50%KAR* condition), to match experimental conditions (Epsztein et al., 2005). We then examined how a single GC responded to inputs arriving within a defined temporal window of integration, mimicking phasic events. To capture the stochastic nature of neuronal activity, each presynaptic input was evoked at a random time within the temporal window. This modelling approach allowed us to independently manipulate two dimensions of the parameter space—namely, the width of the temporal window of integration and the number of GC-GC inputs—parameters that are not experimentally accessible.

We observed that, at 100%AMPAR, small temporal windows were sufficient for successful integration of inputs to generate postsynaptic GC spiking (Fig. 3A1), whereas larger windows were not (Fig. 3B1). In contrast, when synapses operated at 50% KAR, spiking was promoted over broader temporal windows (Fig. 3A2, 3B2). Indeed, larger windows allowed sufficient time for the slow activation of INaP (Fig. 3B2), which was responsible for the sustained amplification and summation of successive incoming KAR-EPSPs. At smaller windows, this mechanism was insufficient to compensate for the smaller amplitude of KAR-EPSPs compared to AMPAR-EPSPs (Fig. 3A2).

We assessed whether that trend was systematic by computing postsynaptic spike probability (Pspk) across 1000 repetitions of the protocol, as a function of the receptor type (either AMPAR or KAR), the window duration, and the number of presynaptic inputs (Fig. 3C1, 3C2). This parametric analysis confirmed initial observations (Artinian et al., 2011). Indeed, for short windows (<30 ms), pure AMPAR-EPSPs (Fig. 3C1) achieved higher spike probabilities than mixed receptor configurations in similar stimulus conditions (Fig. 3C2). Also, it showed that synapses with only AMPARs required fewer inputs than synapses with KARs to trigger postsynaptic spikes. At longer windows (>30 ms), a mixed receptor

composition (50% AMPAR/50% KAR) significantly enhanced postsynaptic spike probability compared to AMPAR-only synapses (compare Fig. 3C1 and 3C2). Under these conditions, mixed-receptor synapses required fewer converging inputs to reach the spike threshold, compared to AMPAR-only synapses.

Globally, this parametric analysis revealed two key findings. First, pure AMPAR-synapses enabled coincidence detection over short windows within the GC network, consistent with the experimental literature on response to perforant path (PP) inputs (Leutgeb et al., 2007; Schmidt-Hieber et al., 2007). More specifically, the model revealed that this coincidence detection was more sensitive in triggering postsynaptic firing, i.e., it required fewer inputs. Second, KAR incorporation extended the temporal window of integration, as found experimentally (Artinian et al., 2011; Epsztein et al., 2010). Moreover, the model unravelled that integration within large temporal windows is again more sensitive, i.e., it requires fewer inputs to generate postsynaptic firing.

The sprouted DG network accounts for the diversity of epileptiform dynamics

We built a detailed biophysical model of the epileptic dentate gyrus (Fig. 4A; see Methods and Supplementary file), using a 1:2000 scaling factor and comprising granule cells (GCs), basket cells (BCs), mossy cells (MCs), and hilar interneurons (HIPPs), endowed with an extended set of ionic channels. Anatomically, the model was organized in a laminar fashion in the septo-temporal dimension (Fig. 4B; z-axis) and extended in the two orthogonal dimensions (x- and y-axes), by considering U-shaped lamella of the DG comprising the different neuronal types, which allowed estimating local field potentials (LFPs, see Fig. 4D-F). Pathological rMF sprouting, i.e. the – level of GC-GC outdegree connectivity – was following a small-world topology, with 5% random connections (Fig. 4C).

We monitored DG network model dynamics in the model following PP stimulation, both by considering spiking activity and estimating LFPs resulting from synaptic currents across all neuronal types, at different laminar levels along the septo-temporal dimension (z-axis, see Fig. 4B). When stimulated, the DG model could produce three distinct types of response (Fig. 4D-F). First, the model displayed sparse spiking in a small subset of GCs and BCs that did not persist beyond PP stimulation (Fig. 4D, top), indicating that this activity was

induced by feed-forward PP inputs and did not imply reverberation within the DG network. This spiking activity resulted in LFPs restricted to a small fraction of channels (Fig. 4D, middle) that were in general flat, compared to those in the two other types of activity (Fig. 4D, bottom).

The two other types of activity were characterized by the recruitment of a much larger fraction of GCs and BCs and the additional activation of MCs and HCs (Fig. 4E and 4F, top). This activity continued well after the termination of the PP stimulation, indicating that it was driven by network reverberation due to recurrent sprouted synapses. Moreover, spiking resulted in LFPs invading all channels (Fig. 4E and 4F, bottom), with typical shapes (Fig. 4G and 4H, top) resembling Interictal Epileptiform Discharges (IEDs) observed experimentally (Fig. 4G and 4H, bottom). Remarkably, while the second type rapidly vanished within a hundred milliseconds after the PP stimulation (Fig. 4E and 4G, top), accounting for transient experimental IEDs (Fig. 4G, bottom), the third type of response displayed reverberating network activity that self-sustained over long periods (Fig. 4F and 4H, top), reproducing long-lasting, sustained, experimental IEDs (Fig. 4I, bottom). Altogether, these observations indicated that the architectural and biophysical constraints considered in the model allowed for the natural emergence of the diversity of network dynamics observed in animal dentate gyri, including distinctive epileptiform activities characterizing hyperexcitable DG network.

KARs broaden the parameter region driving epileptiform activity and enable sustained network hyperexcitability

To investigate how KARs influenced network propensity to generate epileptiform activity (Fig. 4E, F, H, I), we systematically assessed the probability of triggering IEDs, as a function of the parameters setting the timing of PP inputs (window duration) and mossy fiber sprouting (GC-GC outdegree). We hypothesized that KAR-mediated transmission, with its distinct temporal integration properties (as demonstrated at the single-cell level, see Fig. 1-3), would affect the network's ability to generate and maintain IEDs. We assessed this hypothesis by analyzing the IED probability in 100%AMPAR (Fig. 5A) or 50%KAR (Fig. 5B) conditions.

In the 100%AMPAR condition (Fig. 5A), we observed that the IED probability was stronger at short durations, i.e., for PP trains with higher frequency, inducing larger levels of

AMPAR-mediated EPSPs integration, due to their fast kinetics (see Fig. 1-3). Consistently, longer windows impeded the integration of fast AMPAR-mediated EPSPs and decreased the probability of IEDs. Also, increasing network sprouting recurrent connectivity (GC-GC outdegrees > 10-15) raised IED probability, as it favored network reverberation. Moreover, both parameters affected IED probability to similar extents in the ranges considered (i.e., the slope of the 50% IED probability isocline (black dashed line) globally paralleled the first bisectrix). In the 50%KAR condition (Fig. 5B), we found that, contrary to the 100%AMPAR condition, IED probability was less dependent on the duration of the stimulation window (witnessed by a near-horizontal 50% isocline), consistent with the large time constant of KARs that allowed EPSP integration at lower frequencies, compared to AMPAR (see Fig. 1-3). Besides, increasing sprouting connectivity also raised IED probability by increasing the reverberation of network activity.

To better visualize the specific effects of including 50% of KARs, we computed the difference between IED probability maps in their presence versus their absence (Fig. 5C). The resulting representation revealed two parameter regions of interest: a large orange region indicating a higher IED probability when KARs were present, and a small blue region of higher IED probability when only AMPARs were present. The small blue region indicated that triggering IEDs in the 100%AMPAR condition was favored for restricted windows (durations < 30 ms) and low sprouting levels (GC-GC outdegrees ~ 10-15). By contrast, the larger orange region highlighted that KARs shifted the region of higher probability towards longer windows (durations > 60 ms). Noticeably, in this condition, triggering IEDs was strongly favored for a large range of sprouting levels, i.e., whatever the values of GC-GC outdegrees above 15. Overall, while at short window durations, the main factor favoring IEDs was the sprouting level but not the nature of receptors (AMPAR vs KARs), our results revealed that, at longer stimulus durations, the major factor triggering IEDs was the presence of KARs, independently of the sprouting level.

We then evaluated how KARs influence the temporal signature of IEDs, as a means to measure the hyperexcitability of the DG network. We previously identified two distinct temporal signatures of epileptiform activities, i.e., transient (Fig. 4E, H) and sustained (Fig. 4F, I) IEDs, which reflect increasing levels of activity reverberation in the DG epileptic

network. To measure hyperexcitability, we therefore systematically assessed the probability of sustained IEDs (p_{IED}^{sust}; Fig. 5D-E) as a function of the parameters setting the timing of PP inputs (window duration) and network connectivity (GC-GC outdegree), in both 100%AMPAR and 50%KAR conditions.

In the 100%AMPAR condition (Fig. 5D), sustained IEDs were globally very rare, being either absent or appearing at low probability ($p_{IED}^{sust} \sim 0.1 - 0.4$) within a restricted region of the parameter space. Overall, this pattern suggests that under AMPAR-mediated transmission alone, sustained IEDs occur only in a sparse manner across tested conditions. In striking contrast, the presence of KARs (Fig. 5E) resulted in sustained IED that occurred systematically ($p_{IED}^{sust} = 1$) in the vast majority of the parameter space. Noticeably, even at lower sprouting levels (GC-GC outdegrees ~ 10) and shorter stimulation windows (~ 15-45 ms), the network could maintain sustained IEDs, suggesting that the presence of KARs fundamentally enhances network's propensity to encounter lasting pathological activity, a marker of strong hyperexcitability.

Altogether, these findings highlight the crucial role of KARs in both the initiation (Fig. 5A-C) and maintenance (Fig. 5D-E) of epileptiform activity, consistent with previous single-cell (Fig. 1-3) and network (Fig. 4) results. The broader parameter region for IED generation and maintenance in KAR-endowed networks suggests that these receptors act as potent modulators of network hyperexcitability, markedly lowering the threshold for pathological synchronization.

KARs drive a transition from structured to disordered network dynamics

To assess the spatiotemporal organization of sustained interictal epileptiform discharges (IEDs) in the presence or absence of KARs, we first visualized examples of spiking network activity dynamics (Fig. 6A) as orbits in the principal component analysis (PCA) space of GC firing frequencies (Fig. 6B). These orbits were colored as a function of the average topographical position encoded by the GC population's activity. This representation revealed striking differences in collective dynamics between the two conditions. In the 100%AMPA condition, network dynamics orbited along an attractor exhibiting a large and well-structured

shape (Fig. 6B, left) that spanned an extensive range of encoded topographical positions (i.e., blue to red spectrum). Conversely, in the 50%KAR condition (Fig. 6B, right), dynamics revealed an unstructured attractor restricted to a much smaller space region, together with a very limited range of encoded topographical positions (i.e., globally orange). Together, these observations indicated that even under pathological sprouting conditions, the network maintained some degree of organization in its activity in the absence of KARs, while their presence strongly disorganized network activity and topographical encoding.

To better characterize DG dynamics in both conditions, we computed several observables to quantify GCs' activity at the single-neuron level (Fig. 6C-F) and network (Fig. 6G-J) scales, as a function of stimulation window duration and sprouting degree. At the neuronal level, the presence of KARs led to a marked increase in spiking frequency (Fig. 6C). Consistently, KARs induced a significant increase in spiking regularity (Fig. 6D), reflecting a loss of temporal organization in spike trains. Furthermore, the auto-correlation time constant of spiking was decreased in the presence of KARs (Fig. 6E), revealing that this disorganization affected timescales up to the order of a hundred ms. These observations were further confirmed by an increase in entropy, reflecting greater unpredictability (Fig. 6F). At the level of network activity, we found that KARs strongly decreased the synchrony among neighbouring neurons (Fig. 6G), indicative of a disorganization of the spatial structure of activity. Consistently, KARs drastically increased the dimensionality of collective spiking, i.e., more complex dynamics (Fig. 6H). Moreover, the spatial cross-correlation constant of spiking was increased in the presence of KARs (Fig. 6I), indicating that the spatial disorganization of activity arose from more global recurrent interactions across the network. Altogether, the spatial disorganization of activity reduced the mutual information conveyed by collective interactions within the network (Fig. 6J).

In summary, our simulations indicate that KARs profoundly transform IED network dynamics from a partially organized into a highly disordered and complex state. Their presence in the DG networknetwork leads to a breakdown of temporal and spatial organization, generating high-dimensional pathological states with complex dynamics and severely disrupted coordinated activity.

Discussion

The present modeling study unravels the mechanisms by which KARs contribute to epileptogenesis in the DG network, when endowed with aberrant – sprouted – mossy fiber GC-GC connections. We first reveal how the slower time-scale of KARs (vs AMPARs) synaptic integration fundamentally lowers the threshold conditions for network epileptogenesis. Specifically, on the one hand, KARs render the DG network structurally permissive to aberrant activities, by requiring fewer sprouted GC-GC connections to drive epileptiform activities. On the other hand, KARs yield permissivity to aberrant activity in terms of responsiveness, by amplifying network reactivity to external inputs. Consistent with this, KARs have been reported to prolong the duration of epileptiform events recorded in cortical slices from naïve rats under pro-epileptogenic conditions (Szádeczky-Kardoss et al., 2019). We then disclose that, whereas activity is restricted to local and transient spiking patterns under AMPA transmission, KARs induce a state of collective spiking that invades the DG network both in the spatial and temporal domains, under the form of network-wide, sustained, pathological activity. Moreover, this massive propagation is profoundly disorganizing collective spiking, accounting for a large repertoire of interictal activity properties *in vivo*, i.e., lowered temporal synchronization and increased dimensionality of network activity, leading to increased entropy levels and a collapse of mutual information. Altogether, our findings support the view that KARs do not induce a mere quantitative amplification of activity, but rather fundamentally shift the DG network into a different dynamical regime. Our results thus suggest that their presence constitute a consubstantial determinant of the dynamical signature of the sprouted DG, rendering it more permissive and vulnerable to pathological self-sustaining activity. Therefore, KAR-mediated synaptic transmission appears as a critical lever for understanding epileptic DG network dysfunction.

Novelty of the model

The present study aims at assessing how GC–GC sprouted connectivity and the presence of KARs interact to set the threshold and dynamics of epileptiform activities. Probing this structure–function relationship experimentally poses significant challenges, as tools allowing to independently manipulate both the density of sprouted GC–GC synapses and their AMPAR/KAR composition are currently not available in animal models. In this context, modeling represents an essential means to address the question we study. Previous biophysical

models (Morgan et al., 2007; Santhakumar et al., 2005) provided an account of DG activity by including AMPA-mediated excitatory and GABAergic inhibitory synapses. However, they do not account for KAR-mediated transmission at sprouted GC–GC synapses, whereas it has been proved an essential feature of epileptic networks (Baudouin et al., 2024; Boileau et al., 2023; Matsuda et al., 2016; Peret et al., 2014). To address that limitation and to provide a more detailed account of DG activity, we leveraged previous studies to develop an original model incorporating – for the first time – KAR-mediated synaptic transmission at GC–GC sprouted synapses.

Moreover, we endowed the model with several additional novel properties, to further increase the biological relevance of our simulations. For instance, the anatomical description of the DG was improved, with the network being arranged in a multi-layered ring topology reflecting the natural lamellar organization and GC–GC connectivity and with dendrites being spatially oriented. Also, to establish a biophysically constrained implementation of recurrent interactions, we developed a detailed description of AMPAR- and KAR-mediated GC–GC synaptic transmission. Noticeably, the model captured two hallmark KAR properties, relative to AMPARs, i.e., slower decay kinetics and lower maximal conductance, and allowed matching experimentally observed EPSPs of both types. Moreover, GCs were also endowed with the persistent sodium current (INaP), with preferentially amplified KAR- (vs AMPAR-) mediated synaptic transmission, in accordance with experimental observations (Artinian et al., 2011; Baudouin et al., 2024; Boileau et al., 2023; Epsztein et al., 2010, 2005; Matsuda et al., 2016; Peret et al., 2014).

Relevance of the model

The faithful reproduction of experimentally observed synaptic properties provided a critical validation and calibration step of the modelling approach, ensuring that subsequent cellular and network-level simulations were grounded. The model was further validated by the reproduction, at the network scale, of the diversity of collective DG dynamics observed experimentally. Indeed, these LFP responses emerged naturally without any other fitting procedure than that employed at the molecular scale of synaptic receptors, validating the biological realism of the multi-scale modeling approach. The model hence provides a computational framework for dissecting the complex interplay between network architecture, cellular biophysics, and emergent hyperexcitability in epileptic DG, while offering a platform

to test mechanistic hypotheses regarding the differential contributions of synaptic receptor subtypes to epileptogenesis.

KARs transform GC–GC interactions in the sprouted DG

Our previous experimental work has shown that the slow kinetics of KAR-mediated EPSPs support extended temporal summation of synaptic inputs, whereas AMPAR-mediated EPSPs integrate over much narrower windows. Moreover, we previously reported that the recruitment of INaP amplifies the effective integration of EPSPs at larger time scales in the presence of KARs but not AMPARs. These effects resulted in a input-output frequency relationship with a steeper slope (Artinian et al., 2011). Our model was able to account for the effects of the interaction of KAR and INaP currents in broadening the effective integration window, enhancing the summation of successive inputs and driving a larger neuronal gain.

We then assessed how these effects might manifest depending on the context in which the sprouted DG network operates. To accomplish this, we parametrically studied how GCs respond to irregular input patterns within a temporal integration window, thereby emulating the stochastic nature of neuronal spiking that signals phasic events. AMPAR-mediated transmission enabled coincidence detection when inputs were synchronized within short windows, consistent with the established role of GCs as precise temporal filters (Leutgeb et al., 2007; Schmidt-Hieber et al., 2007). By contrast, KARs weakened coincidence detection and enhanced temporal summation at longer time scales, by reducing the number of inputs required to reach threshold. Such transformation of integration properties likely contributes to the breakdown of the dentate gyrus's normal “gatekeeper” function in the epileptic network (Hsu, 2007; Krook-Magnuson et al., 2015), wherein the typically sparse and selective firing of granule cells becomes hyperexcitable and less discriminative.

KARs lower the threshold for DG epileptiform activity

At the network level, the model was able to successfully account for the diversity of DG spiking dynamics, including the simple sparse response to PP inputs, as well as transient or sustained interictal epileptiform discharges (IEDs), as observed experimentally. This showed that, under similar architectural constraints, the dynamical regime of the sprouted DG network was very sensitive to changes in initial conditions or biophysical model parameters. Our systematic exploration of the parameter space governing IED generation revealed that KARs

fundamentally reshape the conditions under which epileptiform activity emerges and persists in recurrent dentate gyrus network.

While AMPAR-only networks exhibited narrow parameter dependencies – requiring precisely timed, high-frequency inputs and moderate sprouting connectivity – the incorporation of KARs dramatically broadened the repertoire of conditions permissive for IED initiation, particularly at longer stimulation windows where slow KAR kinetics enable effective temporal summation.

Most strikingly, KARs transformed the network's propensity for sustained, hyperexcitable activity in the absence of any tonic external drive: whereas the AMPAR-mediated networks rarely maintained prolonged IEDs across the parameter space, KAR-containing networks enabled sufficient levels of activity reverberation to maintain sustained epileptiform discharges under the vast majority of tested conditions, even at lower sprouting levels.

This qualitative shift from sparse, condition-dependent pathological activity to robust, widespread hyperexcitability suggests that KARs do not merely modulate network excitability but rather fundamentally alter the dynamical landscape of the epileptic network. The broadened parameter space for both IED initiation and maintenance suggests that KARs lower thresholds for pathological spiking pattern and enable the network to sustain reverberatory activity across diverse conditions of input stimulations and connectivity configurations.

KARs fundamentally set the dynamical regime of the sprouted DG network

When considering sustained IED, our results demonstrate that KARs do not simply amplify excitation in the sprouted DG network, but rather shift network dynamics into a qualitatively different regime. Indeed, at the single-neuron level, KARs strongly disorganized the temporal structure of activity, with increased spiking regularity, reflecting a loss of patterns in spike trains, shortened autocorrelation time constants, revealing a disorganization at extended timescales and and increased entropy, showing larger unpredictability of the discharge. At the population level, KARs strongly disorganized the spatial structure of activity, reducing local synchrony, increasing the complexity of collective activity, broadening interactions and lowering conveyed mutual information across the network. In summary, our simulations indicated that KARs profoundly transform IED network dynamics from a partially organized state into a highly disordered and complex state. Their presence in the DG network leads to a

breakdown of the temporal and spatial organization, generating high-dimensional pathological states that severely disrupt activity coordination. Mechanistically, we propose that the slow kinetics of KARs sustain elevated firing through temporal summation, thereby stabilizing reverberation and sustained activity, while simultaneously disrupting the precise spike-timing coordination required for structured collective dynamics.

This dual KAR-mediated temporal and spatial reorganization of network dynamics aligns with experimental observations showing that the transition from normal activity to seizure is characterized by a profound qualitative reconfiguration of collective dynamics, rather than an uniform increase in synchrony. The KAR-associated pattern we observe resonates with the canonical progression of focal epilepsy, in which seizures' onset often begin with low-voltage fast activity that is relatively desynchronized before evolving into hypersynchrony activity (Bou Assi et al., 2020; Jiruska et al., 2013; Mormann et al., 2003; Wendling et al., 2003). Moreover, several studies report that dynamical complexity is elevated during interictal-like states yet decreases sharply at the ictal transition (Araújo et al., 2022; Jiruska et al., 2010) again consistent with qualitative shifts in network organization rather than monotonic changes in any single metric.

Taken together, these convergent lines of evidence suggest that KAR-mediated dynamics support a sustained, high-dimensional, desynchronized phase that precedes and facilitates the emergence of seizures. Within this framework, KARs would be pro-epileptogenic in three ways, by (i) lowering the threshold for epileptiform induction, (ii) stabilizing pathological reverberation, and (iii) shifting the network toward more complex, high-dimensional activity patterns, i.e., globally acting as a critical determinant consubstantial with a permissive substrate for seizures.

This interpretation is further supported by several studies demonstrating that selective blockade or reduction of GluK2-containing KARs robustly suppresses seizures in temporal lobe epilepsy models (Baudouin et al., 2024; Boileau et al., 2023; Matsuda et al., 2016; Peret et al., 2014).

Materials and methods

The dentate gyrus network model we built was principally derived from previous modelling and experimental studies (Santhakumar et al., 2005; Morgan et al., 2007; Tejada et al., 2014, 2012; Tejada and Roque, 2014; Yim et al., 2015). The network architecture included four neuronal types, two of them being excitatory – dentate granule cells (GCs) and hilar mossy cells (MCs) – and two inhibitory – dentate basket cells (BCs) and hilar perforant path-associated cells (HCs). It incorporated a 2000:1 scaling of the number of neurons, compared to the rodent dentate gyrus, with 500 GCs, 15 MCs, 6 BCs, and 6 HCs. Each cell type was described as a biophysically realistic multicompartmental model that included a soma and a dendritic tree (containing either 2 or 4 dendrites) and was endowed with multiple ionic and synaptic conductances. The multicompartmental architecture, intrinsic and synaptic modelled properties, based on specific morphological and electrophysiological data of the four cell types reported in the literature, as well as the procedures for estimating local field potentials and activity observables can be found in the Supplementary File. The model was simulated in the NEURON environment (Hines and Carnevale, 1997).

Acknowledgements

We thank Alfonso Represa for helpful comments and discussions.

Additional information

Funding

This work was supported by the Institut National de la Santé et de la Recherche Médicale (INSERM), Aix-Marseille University (AMU), the Agence Nationale de la Recherche (ANR-18-CE17-0023-01) to VC, and Sorbonne University (Paris) to BD.

Author contributions

VC designed the original architecture of the project. VC and LGL designed the study of dentate gyrus cellular aspects. VC, BD and LGL designed the study of dentate gyrus network aspects. LGL built and simulated the model. PB and MA supervised and LGL achieved the study of local field potentials. BD supervised, and BD and LGL achieved the analysis of the network activity. VC and BD wrote the manuscript with contributions from LGL and feedbacks from PB and MA.

Authors ORCIDS

Valérie Crépel ID: https://orcid.org/0000-0003-0408-3766

Bruno Delord ID: https://orcid.org/0000-0002-2912-3405

Data availability

Modeling results were generated via a custom-made MATLAB/Python code available through GitHub. The experimental data used in the present study were previously published in Epsztein et al. (2010) and Artinian et al. (2011) as indicated in the text and figures.

Declaration of Competing Interest

This work was supported exclusively by academic funding. VC had filed patents that are not related to this study and had received support from uniQure, which had no involvement in the present study. The remaining authors (LGL, PB, MA, BD) declare no conflicts of interest.

References

Araújo NS, Reyes-Garcia SZ, Brogin JAF, Bueno DD, Cavalheiro EA, Scorza CA, Faber J. 2022. Chaotic and stochastic dynamics of epileptiform-like activities in sclerotic hippocampus resected from patients with pharmacoresistant epilepsy. PLOS Computational Biology **18**:e1010027. DOI: https://doi.org/10.1371/journal.pcbi.1010027

Artinian J, Peret A, Marti G, Epsztein J, Crepel V. 2011. Synaptic Kainate Receptors in Interplay with INaP Shift the Sparse Firing of Dentate Granule Cells to a Sustained Rhythmic Mode in Temporal Lobe Epilepsy. Journal of Neuroscience **31**:10811–10818. DOI: https://doi.org/10.1523/JNEUROSCI.0388-11.2011

Artinian J, Peret A, Mircheva Y, Marti G, Crépel V. 2015. Impaired neuronal operation through aberrant intrinsic plasticity in epilepsy: Aberrant Intrinsic Plasticity. Annals of Neurology **77**:592–606. DOI: https://doi.org/10.1002/ana.24348

Baudouin SJ, Giles A, Pearson N, Deforges S, He C, Boileau C, Partouche N, Borta A, Gautron J, Wartel M, Bočkaj I, Scavarda D, Bartolomei F, Penchet G, Aupy J, Sims J, Smith J, Mercer A, Danos O, Mulle C, Crépel V, Porter R. 2024. A novel AAV9-dual microRNA- vector targeting *GRIK2* in the hippocampus as a treatment for mesial temporal lobe epilepsy. Molecular Therapy - Methods & Clinical Development 101342. DOI: https://doi.org/10.1016/j.omtm.2024.101342

Boileau C, Deforges S, Peret A, Scavarda D, Bartolomei F, Giles A, Partouche N, Gautron J, Viotti J, Janowitz H, Penchet G, Marchal C, Lagarde S, Trebuchon A, Villeneuve N, Rumi J, Marissal T, Khazipov R, Khalilov I, Martineau F, Maréchal M, Lepine A, Milh M, Figarella-Branger D, Dougy E, Tong S, Appay R, Baudouin S, Mercer A, Smith JB, Danos O, Porter R, Mulle C, Crépel V. 2023. GluK2 Is a Target for Gene Therapy in Drug-Resistant Temporal Lobe Epilepsy. Annals of Neurology. DOI: https://doi.org/10.1002/ana.26723, PMID: 37341588

Bou Assi E, Zerouali Y, Robert M, Lesage F, Pouliot P, Nguyen DK. 2020. Large-Scale Desynchronization During Interictal Epileptic Discharges Recorded With Intracranial EEG. Frontiers in Neurology **11**:529460. DOI: https://doi.org/10.3389/fneur.2020.529460

Buckmaster PS. 2012. Mossy Fiber Sprouting in the Dentate Gyrus. Jasper's Basic Mechanisms of the Epilepsies.

Epsztein J, Represa A, Jorquera I, Ben-Ari Y, Crépel V. 2005. Recurrent mossy fibers establish aberrant kainate receptor-operated synapses on granule cells from epileptic rats. The Journal of Neuroscience: The Official Journal of the Society for Neuroscience **25**:8229–8239. DOI: https://doi.org/10.1523/JNEUROSCI.1469-05.2005, PMID: 16148230

Epsztein J, Sola E, Represa A, Ben-Ari Y, Crépel V. 2010. A Selective Interplay between Aberrant EPSPKA and INaP Reduces Spike Timing Precision in Dentate Granule Cells of Epileptic Rats. Cerebral Cortex **20**:898–911. DOI: https://doi.org/10.1093/cercor/bhp156

Gabriel S. 2004. Stimulus and Potassium-Induced Epileptiform Activity in the Human Dentate Gyrus from Patients with and without Hippocampal Sclerosis. Journal of Neuroscience **24**:10416–10430. DOI: https://doi.org/10.1523/JNEUROSCI.2074-04.2004

Goirand-Lopez L, Moulinier M, Vigier A, Boileau C, Carleton A, Muldoon SF, Marissal T, Crépel V. 2023. Kainate receptors modulate the microstructure of synchrony during

dentate gyrus epileptiform activity. Neurobiology of Disease **185**:106260. DOI: https://doi.org/10.1016/j.nbd.2023.106260

Helmstaedter C, Al-Haj Mustafa S, Witt J-A. 2025. Temporal trends indicate an epidemiological shift in the pathology of mesial temporal lobe epilepsy. Journal of Neurology **272**:652. DOI: https://doi.org/10.1007/s00415-025-13398-1, PMID: 40993433

Hines ML, Carnevale NT. 1997. The NEURON simulation environment. Neural Computation **9**:1179–1209. DOI: https://doi.org/10.1162/neco.1997.9.6.1179, PMID: 9248061

Hsu D. 2007. The dentate gyrus as a filter or gate: a look back and a look ahead. *Progress in Brain Research*. Elsevier. p. 601–613. DOI: https://doi.org/10.1016/S0079-6123(07)63032-5

Jiruska P, Csicsvari J, Powell AD, Fox JE, Chang W-C, Vreugdenhil M, Li X, Palus M, Bujan AF, Dearden RW, Jefferys JGR. 2010. High-Frequency Network Activity, Global Increase in Neuronal Activity, and Synchrony Expansion Precede Epileptic Seizures In Vitro. Journal of Neuroscience **30**:5690–5701. DOI: https://doi.org/10.1523/JNEUROSCI.0535-10.2010, PMID: 20410121

Jiruska P, de Curtis M, Jefferys JGR, Schevon CA, Schiff SJ, Schindler K. 2013. Synchronization and desynchronization in epilepsy: controversies and hypotheses. The Journal of Physiology **591**:787–797. DOI: https://doi.org/10.1113/jphysiol.2012.239590, PMID: 23184516

Krook-Magnuson E, Armstrong C, Bui A, Lew S, Oijala M, Soltesz I. 2015. *In vivo* evaluation of the dentate gate theory in epilepsy: Dentate gate in temporal lobe epilepsy. The Journal of Physiology **593**:2379–2388. DOI: https://doi.org/10.1113/JP270056

Lee J. 2007. Fast Rhythmic Bursting Cells: The Horizontal Fiber System in the Cat's Primary Visual Cortex.

Leutgeb JK, Leutgeb S, Moser M-B, Moser EI. 2007. Pattern Separation in the Dentate Gyrus and CA3 of the Hippocampus. Science **315**:961–966. DOI: https://doi.org/10.1126/science.1135801

Matsuda K, Budisantoso T, Mitakidis N, Sugaya Y, Miura E, Kakegawa W, Yamasaki M, Konno K, Uchigashima M, Abe M, Watanabe I, Kano M, Watanabe M, Sakimura K, Aricescu AR, Yuzaki M. 2016. Transsynaptic Modulation of Kainate Receptor Functions by C1q-like Proteins. Neuron **90**:752–767. DOI: https://doi.org/10.1016/j.neuron.2016.04.001

Morgan RJ, Santhakumar V, Soltesz I. 2007. Modeling the dentate gyrus. *Progress in Brain Research*. Elsevier. p. 639–658. DOI: https://doi.org/10.1016/S0079-6123(07)63035-0

Mormann F, Kreuz T, Andrzejak RG, David P, Lehnertz K, Elger CE. 2003. Epileptic seizures are preceded by a decrease in synchronization. Epilepsy Research **53**:173–185. DOI: https://doi.org/10.1016/S0920-1211(03)00002-0

Peret A, Christie LA, Ouedraogo DW, Gorlewicz A, Epsztein J, Mulle C, Crépel V. 2014. Contribution of Aberrant GluK2-Containing Kainate Receptors to Chronic Seizures in Temporal Lobe Epilepsy. Cell Reports **8**:347–354. DOI: https://doi.org/10.1016/j.celrep.2014.06.032

Represa A, Le Gall La Salle G, Ben-Ari Y. 1989. Hippocampal plasticity in the kindling model of epilepsy in rats. Neuroscience Letters **99**:345–350. DOI: https://doi.org/10.1016/0304-3940(89)90471-0

Santhakumar V, Aradi I, Soltesz I. 2005. Role of mossy fiber sprouting and mossy cell loss in hyperexcitability: a network model of the dentate gyrus incorporating cell types and axonal topography. Journal of Neurophysiology **93**:437–453. DOI: https://doi.org/10.1152/jn.00777.2004, PMID: 15342722

Schmidt-Hieber C, Jonas P, Bischofberger J. 2007. Subthreshold dendritic signal processing and coincidence detection in dentate gyrus granule cells. The Journal of Neuroscience: The Official Journal of the Society for Neuroscience **27**:8430–8441. DOI: https://doi.org/10.1523/JNEUROSCI.1787-07.2007, PMID: 17670990

Sutula T, Cascino G, Cavazos J, Parada I, Ramirez L. 1989. Mossy fiber synaptic reorganization in the epileptic human temporal lobe. Annals of Neurology **26**:321–330. DOI: https://doi.org/10.1002/ana.410260303

Szádeczky-Kardoss K, Varró P, Szűcs A, Borbély S, Világi I. 2019. Kainate receptors have different modulatory effect in seizure-like events and slow rhythmic activity in entorhinal cortex ex vivo. Brain Research Bulletin **153**:279–288. DOI: https://doi.org/10.1016/j.brainresbull.2019.09.009

Tejada J, Arisi GM, García-Cairasco N, Roque AC. 2012. Morphological alterations in newly born dentate gyrus granule cells that emerge after status epilepticus contribute to make them less excitable. PloS One **7**:e40726. DOI: https://doi.org/10.1371/journal.pone.0040726, PMID: 22811762

Tejada J, Garcia-Cairasco N, Roque AC. 2014. Combined role of seizure-induced dendritic morphology alterations and spine loss in newborn granule cells with mossy fiber sprouting on the hyperexcitability of a computer model of the dentate gyrus. PLoS computational biology **10**:e1003601. DOI: https://doi.org/10.1371/journal.pcbi.1003601, PMID: 24811867

Tejada J, Roque AC. 2014. Computational models of dentate gyrus with epilepsy-induced morphological alterations in granule cells. Epilepsy & Behavior **38**:63–70. DOI: https://doi.org/10.1016/j.yebeh.2014.02.007

Téllez-Zenteno JF, Hernández-Ronquillo L. 2012. A Review of the Epidemiology of Temporal Lobe Epilepsy. Epilepsy Research and Treatment **2012**:1–5. DOI: https://doi.org/10.1155/2012/630853

Wendling F, Bartolomei F, Bellanger JJ, Bourien J, Chauvel P. 2003. Epileptic fast intracerebral EEG activity: evidence for spatial decorrelation at seizure onset. Brain: A Journal of Neurology **126**:1449–1459. DOI: https://doi.org/10.1093/brain/awg144, PMID: 12764064

Yim MY, Hanuschkin A, Wolfart J. 2015. Intrinsic rescaling of granule cells restores pattern separation ability of a dentate gyrus network model during epileptic hyperexcitability: INTRINSIC RESCALING AND NEURONAL NETWORK PATTERN SEPARATION. Hippocampus **25**:297–308. DOI: https://doi.org/10.1002/hipo.22373

Figure legends

Fig. 1. Comparison of AMPA- and Kainate Receptor-Mediated Excitatory Postsynaptic Potentials Derived from Computational Modeling and Experimental Recordings. Comparative traces of AMPA (black) and kainate (KA, red) receptor-mediated excitatory postsynaptic potentials (EPSPs) obtained from computational modeling (mEPSP; A1, B1), derived (δ) from patch-clamp recordings of simulated EPSPs generated by somatic current injections (simulated EPSP; A2) and EPSPs evoked by electrical stimulation (evoked EPSP; B2), from Epsztein et al. (2010). Traces depict EPSPs at resting membrane potential (Vrest) and depolarized subthreshold potentials. Note that computational models (A1, B1) accurately reproduce the fast and slow kinetics of AMPAR-EPSPs and KAR-EPSPs observed in experimental recordings (A2, B2). Notably, mEPSP_KA exhibits more pronounced subthreshold potential amplification compared to mEPSP_AMPA, as observed under experimental conditions, demonstrating the reliability of the computational model-based approach in capturing synaptic signal dynamics.

Fig. 2. Comparison of AMPA-EPSP and KA-EPSP Integration and Firing Dynamics Following a Train of Stimulation Derived from Computational Modeling and Experimental Recordings. A1-A2, Comparative traces of trains of AMPAR-EPSP (black) and KAR-EPSP (red) obtained from computational modeling (mEPSP, A1) and derived from patch-clamp recordings (eEPSP, A2) from Artinian et al. (2011). Traces depict trains of EPSPs evoked at 30 Hz at resting membrane potential (Vrest) and depolarized subthreshold potentials with and without persistent sodium current (INaP). Note that computational models accurately reproduce the dynamics of integration of KAR-EPSP and AMPAR-EPSP observed in experimental recordings. Notably, KAR-mEPSP exhibit more pronounced subthreshold potential amplification due to INaP compared to AMPAR-mEPSP, as observed under experimental conditions, demonstrating the reliability of the computational modeling in capturing the dynamics of synaptic response integration. B1-B2, Comparative spike discharge for AMPAR- (black) and KAR- (red) mEPSPs evoked at 30 Hz and obtained from computational modeling (B1) and patch-clamp recordings (eEPSP, B2) from Artinian et al. (2011). Note that computational models accurately reproduce the differential firing patterns, as observed under experimental conditions, demonstrating a higher spike discharge generated by KAR-mEPSP compared to AMPAR-mEPSP. C1-C2, Input-output relationship

demonstrating firing rate modulation as a function of input frequency, derived from computational modeling (C1) and patch-clamp recordings (C2) from Artinian et al. (2011). Note that computational models accurately replicate the distinct coefficients of AMPAR-mEPSP and KAR-mEPSP, as observed in patch-clamp recordings. This underscores the reliability of the computational approach in capturing input-driven firing dynamics.

Fig. 3. Differential Temporal Integration of Synaptic Inputs by AMPAR-only versus Mixed AMPAR/KAR Synapses. (A1–B1) represent conditions with 100% AMPAR, while (A2–B2) correspond to conditions with 50% AMPAR and 50% KAR. (A1) Example of stimulation of 8 GC inputs within a 10 ms window (top trace), inducing summation of EPSPs and leading to spike generation (bottom trace; also marked by star in C1). (B1) Example of stimulation of 12 GC inputs within a 100 ms window (top trace), inducing summation of EPSPs but failing to trigger spike generation (bottom trace; also marked by circle in C1). (A2) Example of stimulation of 8 inputs within a 10 ms window (top trace), inducing summation of EPSPs but failing to trigger spike generation (bottom trace; marked by circle in C2). (B2) Example of stimulation of 12 inputs within a 100 ms window (top trace), inducing summation of EPSPs and leading to spike generation (bottom trace; also marked by star in C2). Across all trials, each stimulation was randomly selected with uniform probability within the specified time window. (C1–C2) Heatmaps representing the probability of spiking (P_spk) as a function of the number of inputs (GC-GC indegree) and the stimulation window duration. C1 corresponds to 100% AMPAR, whereas C2 represents 50% AMPAR and 50% KAR conditions. In the presence of 100% AMPAR, a low number of inputs is sufficient to trigger a spike within a narrow time window (star), but when the stimulation window is expanded, the probability of spiking is strongly reduced even when the number of inputs is increased (circle). In contrast, under 50% AMPAR and 50% KAR conditions, a low number of inputs fails to trigger a spike in a narrow window (circle), but the probability of spiking becomes high with a broader time window and a moderate number of inputs (star).

Fig. 4. Dentate Gyrus Network Model: Structure, Topology, and Activity Patterns. (A) Schematic representation of the dentate gyrus (DG) network model illustrating cell types—500 granule cells (GC), 15 mossy cells (MC, shown in orange), 6 basket cells (BC, shown in red), and 6 HIPP cells (HC, shown in green) – together with their connectivity and distribution across the three main layers: Molecular Layer, Granule Cell Layer, and Hilus. The

output degree (number of synapses onto target neurons) is indicated next to each connection type. The number of recurrent mossy fiber (rMF) connections (nrMF) is a key model parameter varying with the degree of mossy fiber sprouting. (B) Three-dimensional spatial organization of the model network, showing the anatomical localization of all neuron types. The schematic highlights representative examples of the cell types included in the computational DG model. (C) Schematic representation of the recurrent mossy fiber (rMF) small-world network topology characteristic of the epileptic dentate gyrus network. (D–F) Network responses to 10 phasic perforant path (PP, upward deflection) single input stimulations within a 60 ms time window, at 16% sprouting level, and with a mixed receptor composition (50% AMPA, 50% kainate), displaying three distinct activity patterns. Stimulation of the DG network was achieved by applying one PP spike to 1-2% of the 500 GCs and 1-2 PP spikes in each of the 6 BCs on average, with adapted synaptic weights so that a single presynaptic spike elicited a postsynaptic spike. Each panel comprises: raster plots of neuronal firing (#Cells) over time for each cell type (GC, MC, BC, HIPP) (top); multi-channel (1–11) recordings of network activity (middle); and local field potential derived from computational modeling (mLFP) alongside experimental EEG (eEEG) traces (bottom). Panel D shows minimal network response with brief activation restricted to a few cells (sparse activity). Panel E demonstrates a transient network response with temporary, widespread activation across cell types. Panel F illustrates a sustained network response with persistent activity involving all cell populations. (G-I) Examples of mLFP (blue traces) in conditions of sparse activity (G), and transient (H) or sustained (I) IEDs. Note that simulated IEDs display similar waveforms to those of IEDs digitized (500 Hz) from experimental EEG recordings in the hippocampus of chronic epileptic mice. This model faithfully recapitulates both the anatomical organization of the dentate gyrus and the range of activity patterns observed experimentally.

Fig. 5. Distinct Probability of Generating Transient and Sustained IEDs Depending on the Presence of AMPAR-only and Mixed AMPAR/KAR Receptor Conditions. (A-B), The heatmaps illustrate the probability of generating Interictal Epileptiform Discharges (IEDs) under two distinct synaptic receptor conditions: 100% AMPA receptors (A) and mixed receptor composition of 50% AMPA and 50% kainate receptors (B). Each heatmap plots the duration of the stimulation window (x-axis, 0-105 ms with 15 ms step) versus the percentage of recurrent mossy fiber (rMF) sprouting (y-axis, 10-31% with 3% step). The color intensity

represents the probability of IED ($P_{IEDs)}$ generation in response to phasic stimulation of 10 perforant path inputs distributed across the different stimulation time windows. The 0.5 isocline (black curve) indicates the boundary where the probability of IED generation is 50%. C, The heatmap results from the difference between the heatmap with mixed (50% AMPAR/50% KAR) and the heatmap with 100% AMPAR shown in (A) and (B), respectively. This heatmap highlights specific regions of differential activity. Positive values (orange) indicate enhanced epileptiform activity generation probability with mixed receptors for longer stimulation windows across a wide range of sprouting percentages. In contrast, negative values (blue) reveal that the pure AMPAR condition shows more specific pathlogocial activity restricted to brief stimulations and low sprouting. Black areas represent equal activity levels for both conditions. (D-E), Under the same synaptic receptor conditions and graphical representation, these heatmaps show the probability of sustained IEDs. The color intensity now represents the probability of generating sustained epileptiform activity in response to the same stimulation protocol. Note there is a low probability to generate sustained IEDs in the presence of 100% AMPAR in contrast to the condition with 50% AMPAR and 50% KAR.

Fig. 6. Kainate receptors shift the spatio-temporal landscape of sustained IEDs towards high-dimensional and complex network dynamics. (A) Representative spiking raster plots showing sustained network activity under two synaptic receptor conditions: 100% AMPA receptors (left) and 50% AMPA/50% kainate receptors (right). Each plot displays neuronal firing (#Cells) over time for different cell types (GC, MC, BC, HIPP) following 10 phasic perforant path (PP) stimulations (upward deflections) within a 30 ms window under 25% sprouting conditions . The mixed AMPAR/KAR condition shows strikingly different temporal dynamics compared to pure AMPAR. (B) PCA visualization of firing frequency trajectories under both receptor conditions. Colors represent average topographic position encoded by granule cell activity (blue to red spectrum). The 100% AMPAR condition (left) shows structured attractor dynamics with large topographic range (full color spectrum), while 50% AMPAR/50% KAR (right) displays complex, unstructured patterns with reduced range (predominantly orange). (C-J) Maps of activity observables at the neuron– (C-F) and network– (G-J) levels under both receptor conditions: (C) mean spiking frequency, (D)

spiking irregularity (CV2), (E) auto-correlation time constant, (F) entropy, (G) synchrony, (H) dimensionality (a.u.), (I) cross-correlation space constant, (J) mutual information.

Fig. 1

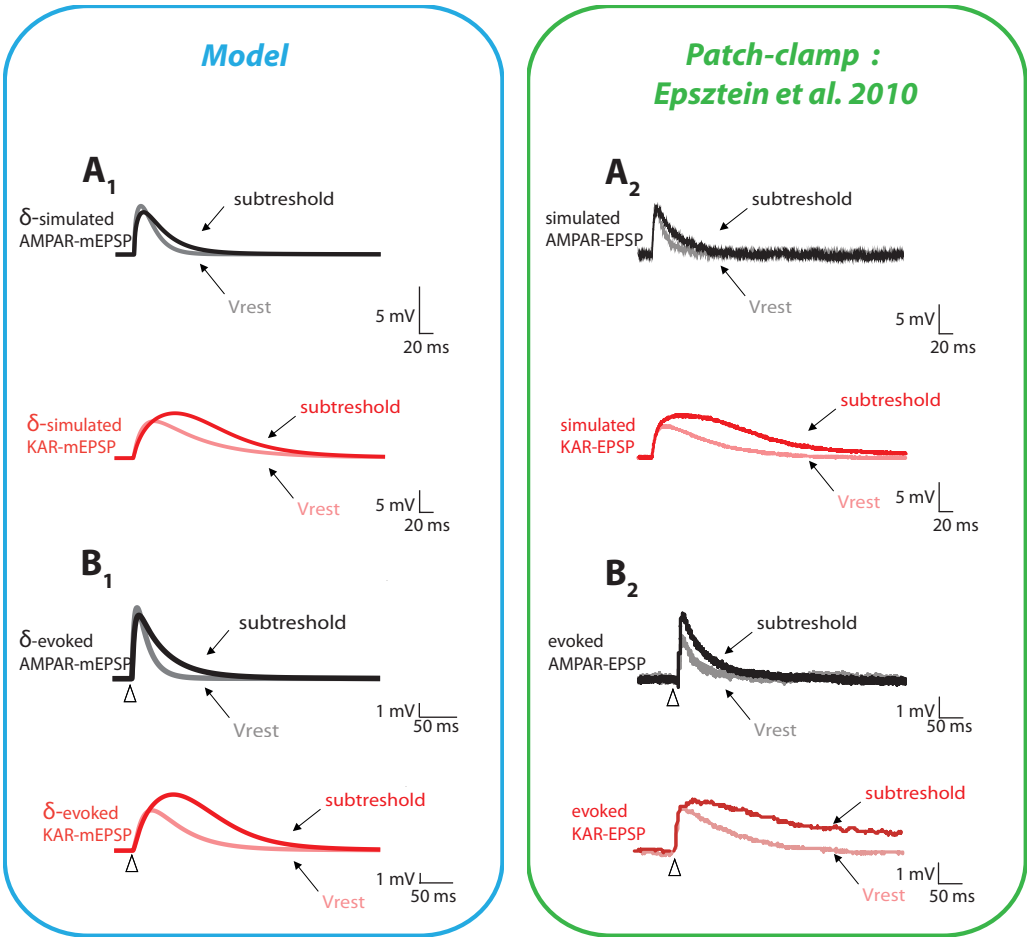
Model
A1
δ-simulated
AMPAR-mEPSP
subtreshold
Vrest
5 mV
20 ms
δ-simulated
KAR-mEPSP
subtreshold
Vrest
5 mV
20 ms
B1
δ-evoked
AMPAR-mEPSP
subtreshold
Vrest
1 mV
50 ms
δ-evoked
KAR-mEPSP
subtreshold
Vrest
1 mV
50 ms
Patch-clamp :
Epsztein et al. 2010
A2
simulated
AMPAR-EPSP
subtreshold
Vrest
5 mV
20 ms
simulated
KAR-EPSP
subtreshold
Vrest
5 mV
20 ms
B2
evoked
AMPAR-EPSP
subtreshold
Vrest
1 mV
50 ms
evoked
KAR-EPSP
subtreshold
Vrest
1 mV
50 ms

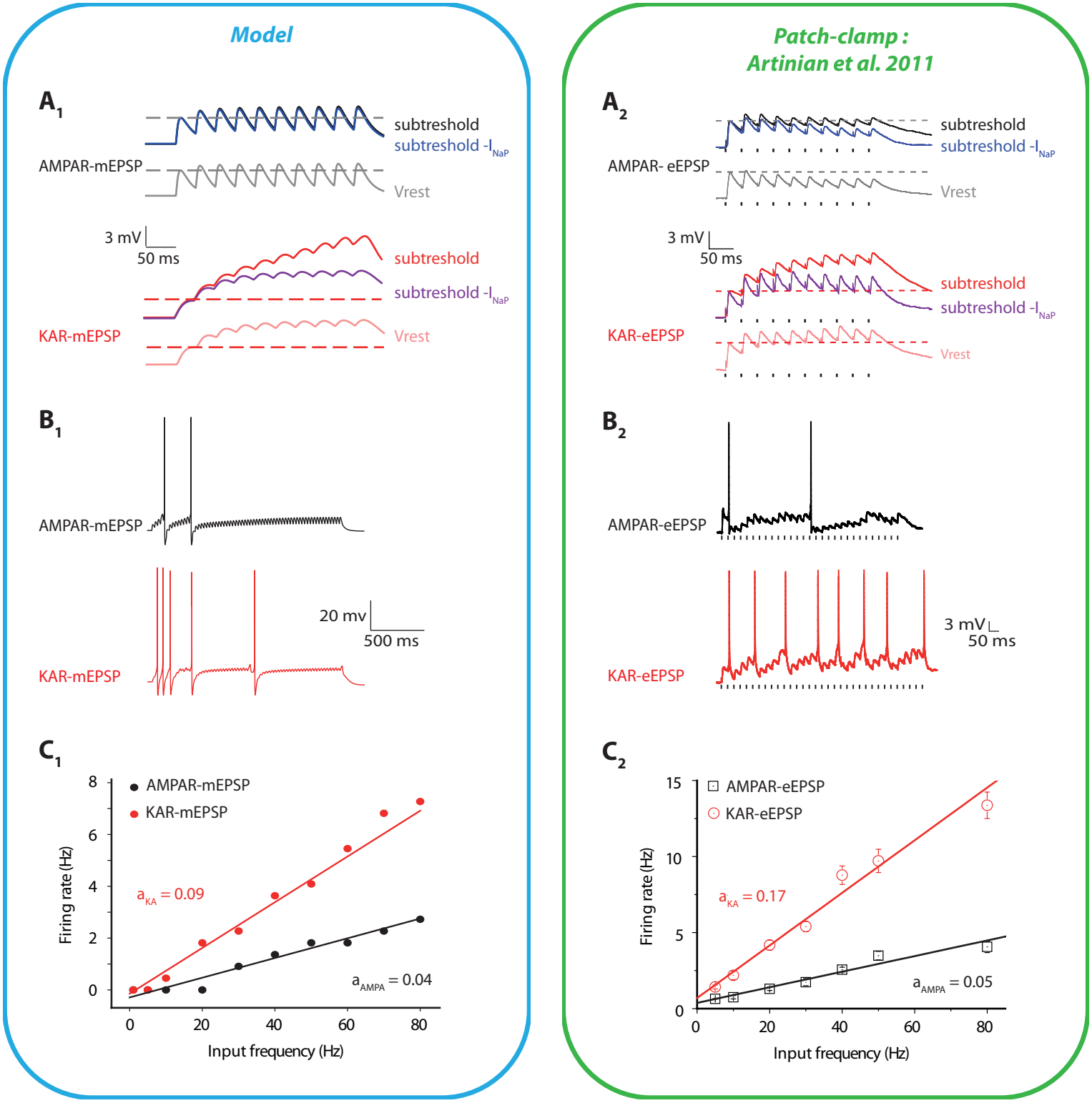
Model
A1
AMPAR-mEPSP
subtreshold
subtreshold -INaP
Vrest
3 mV
50 ms
KAR-mEPSP
subtreshold
subtreshold -INaP
Vrest
B1
AMPAR-mEPSP
20 mv
500 ms
KAR-mEPSP
C1
AMPAR-mEPSP
KAR-mEPSP
aKA = 0.09
aAMPA = 0.04
Firing rate (Hz)
Input frequency (Hz)
Patch-clamp :
Artinian et al. 2011
A2
AMPAR- eEPSP
subtreshold
subtreshold -INaP
Vrest
3 mV
50 ms
KAR-eEPSP
subtreshold
subtreshold -INaP
Vrest
B2
AMPAR-eEPSP
3 mV
50 ms
KAR-eEPSP
C2
AMPAR-eEPSP
KAR-eEPSP
aKA = 0.17
aAMPA = 0.05
Firing rate (Hz)
Input frequency (Hz)

Fig. 3

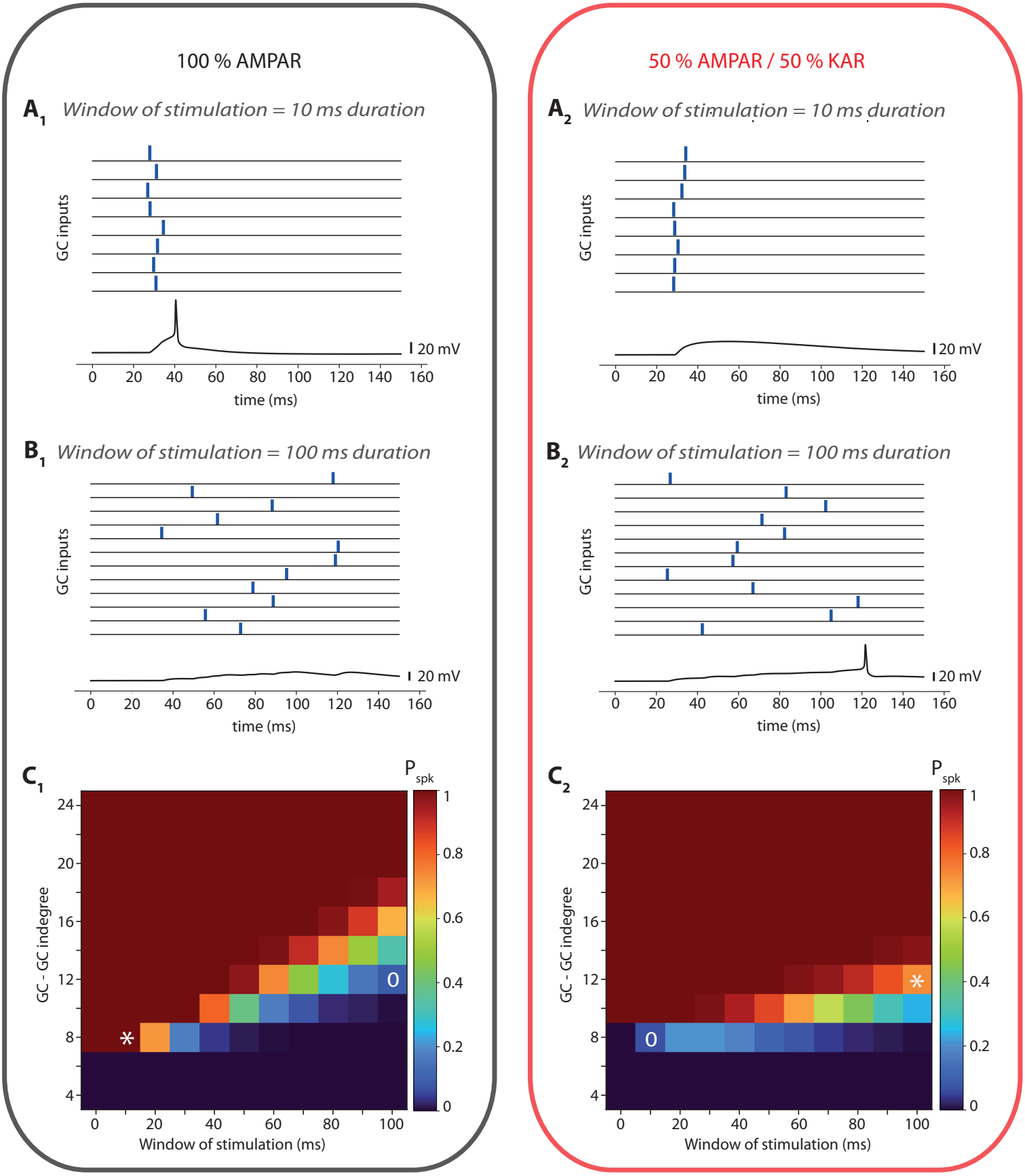
100 % AMPAR
A1 Window of stimulation = 10 ms duration
GC inputs
20 mV
0 20 40 60 80 100 120 140 160
time (ms)
B1 Window of stimulation = 100 ms duration
GC inputs
20 mV
0 20 40 60 80 100 120 140 160
time (ms)
C1
Pspk
1
0.8
0.6
0.4
0.2
0
GC - GC indegree
24
20
16
12
8
4
0 20 40 60 80 100
Window of stimulation (ms)
50 % AMPAR / 50 % KAR
A2 Window of stimulation = 10 ms duration
GC inputs
20 mV
0 20 40 60 80 100 120 140 160
time (ms)
B2 Window of stimulation = 100 ms duration
GC inputs
20 mV
0 20 40 60 80 100 120 140 160
time (ms)
C2
Pspk
1
0.8
0.6
0.4
0.2
0
GC - GC indegree
24
20
16
12
8
4
0 20 40 60 80 100
Window of stimulation (ms)

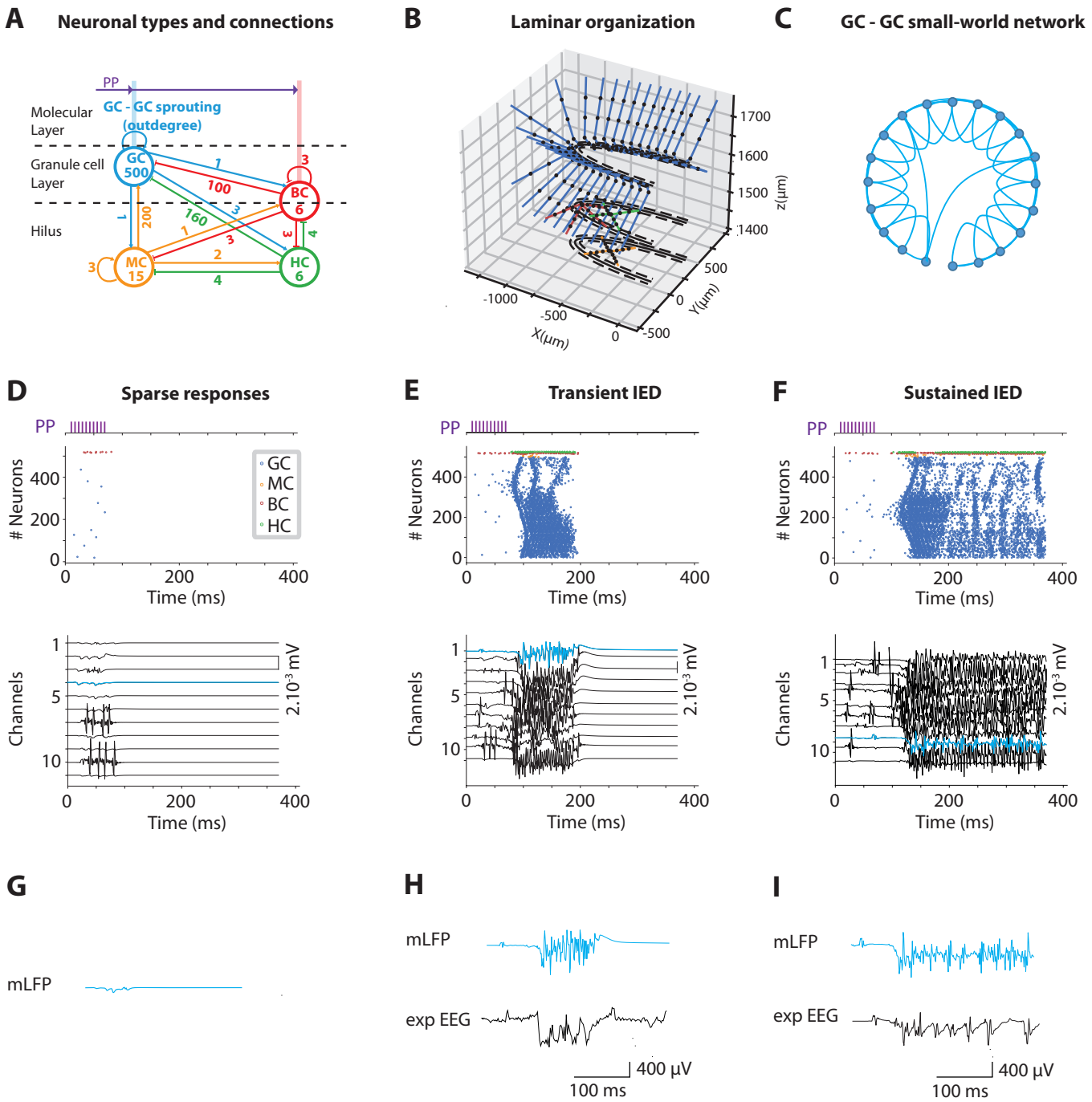
A
Neuronal types and connections
PP
GC - GC sprouting
(outdegree)
Molecular Layer
Granule cell Layer
Hilus
GC 500
BC 6
MC 15
HC 6
B
Laminar organization
z(µm)
Y(µm)
X(µm)
C
GC - GC small-world network
D
Sparse responses
E
Transient IED
F
Sustained IED
Neurons
Time (ms)
Channels
2.10-3 mV
GC
MC
BC
HC
G
mLFP
H
mLFP
exp EEG
400 µV
100 ms
I
mLFP
exp EEG
400 µV
100 ms

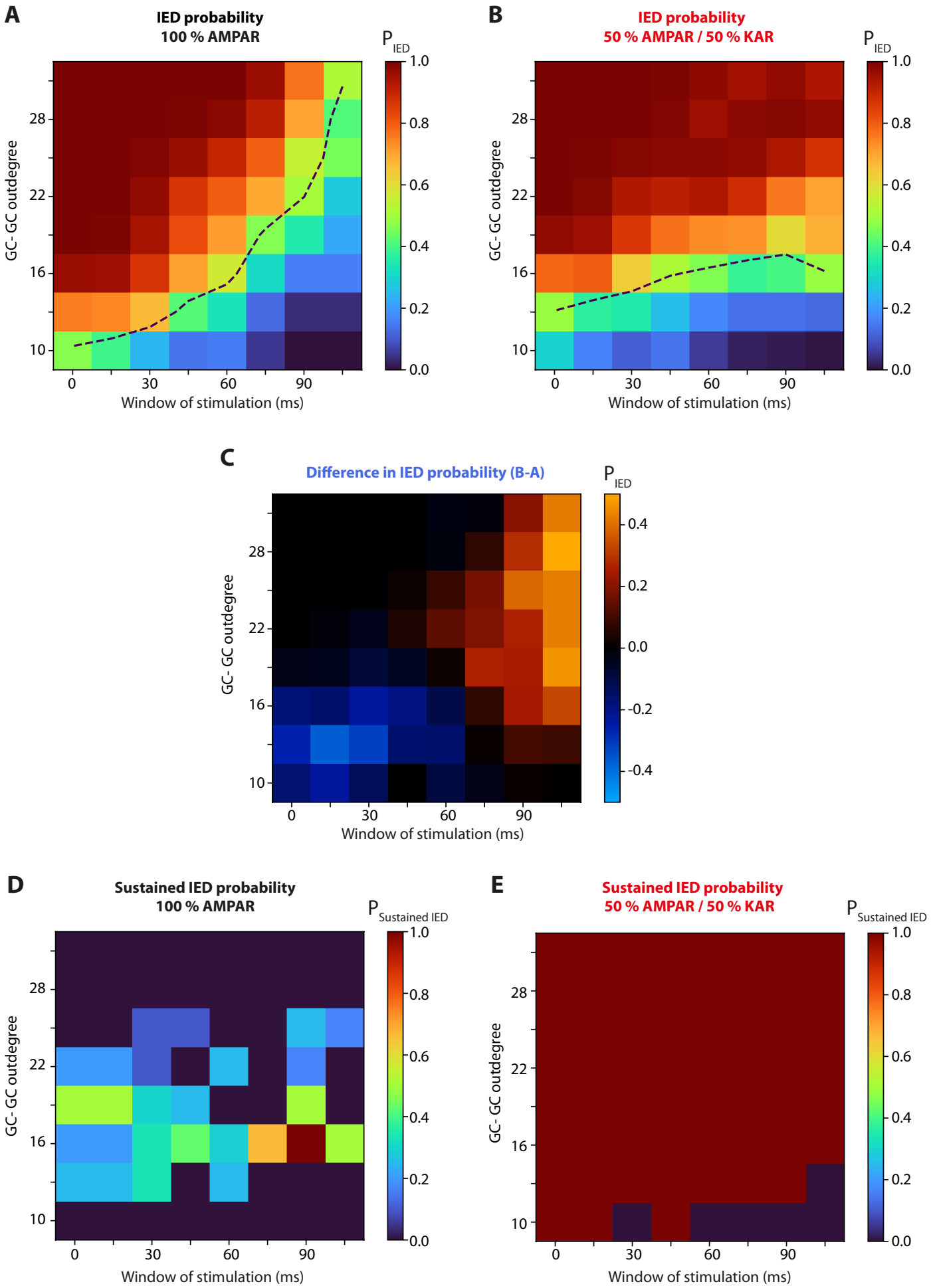
A
IED probability
100 % AMPAR
P IED
1.0
0.8
0.6
0.4
0.2
0.0
GC- GC outdegree
28
22
16
10
0
30
60
90
Window of stimulation (ms)
B
IED probability
50 % AMPAR / 50 % KAR
P IED
1.0
0.8
0.6
0.4
0.2
0.0
GC- GC outdegree
28
22
16
10
0
30
60
90
Window of stimulation (ms)
C
Difference in IED probability (B-A)
P IED
0.4
0.2
0.0
-0.2
-0.4
GC- GC outdegree
28
22
16
10
0
30
60
90
Window of stimulation (ms)
D
Sustained IED probability
100 % AMPAR
P Sustained IED
1.0
0.8
0.6
0.4
0.2
0.0
GC- GC outdegree
28
22
16
10
0
30
60
90
Window of stimulation (ms)
E
Sustained IED probability
50 % AMPAR / 50 % KAR
P Sustained IED
1.0
0.8
0.6
0.4
0.2
0.0
GC- GC outdegree
28
22
16
10
0
30
60
90
Window of stimulation (ms)

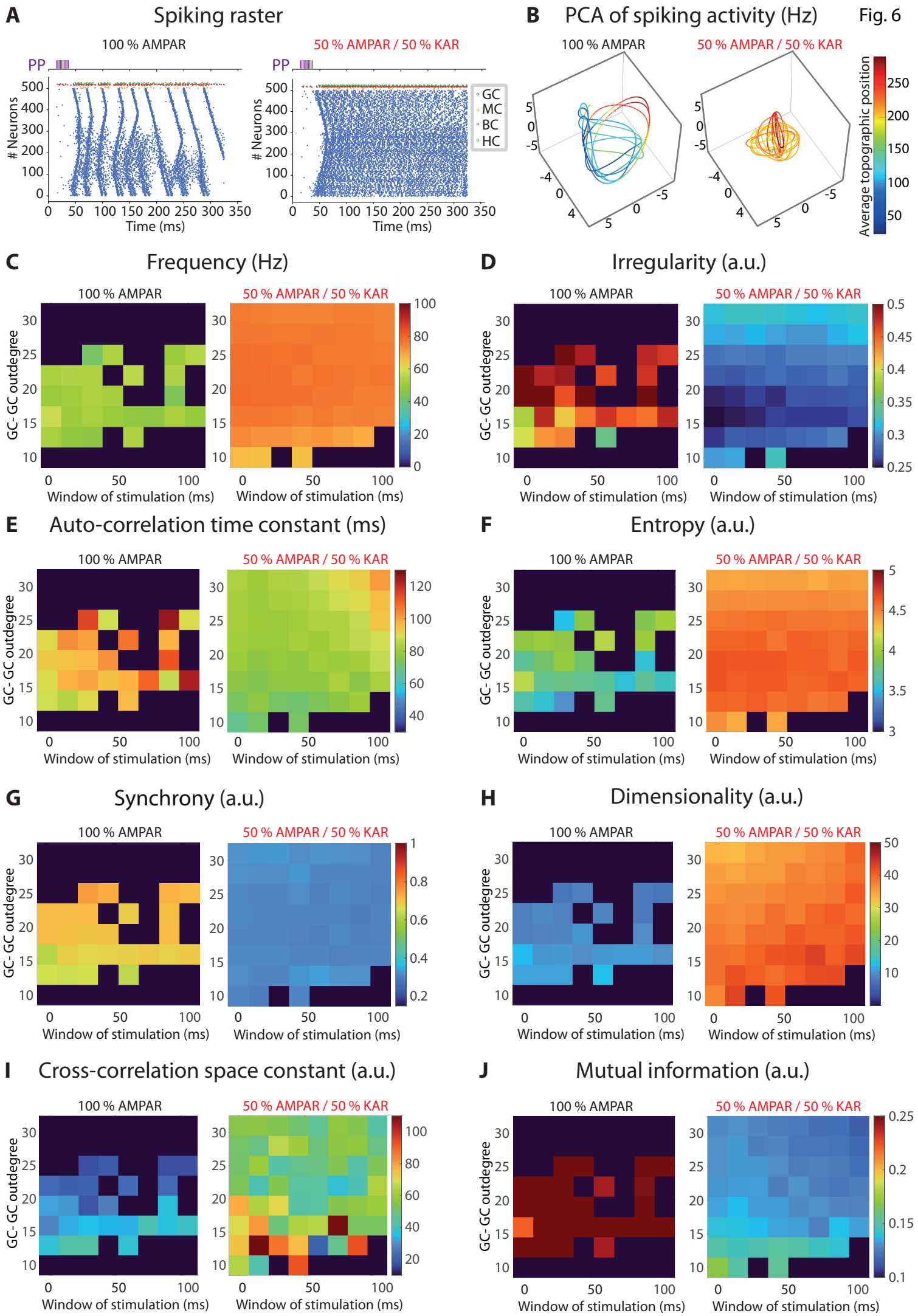
Fig. 6
A
Spiking raster
100 % AMPAR
50 % AMPAR / 50 % KAR
PP
Neurons
Time (ms)
GC
MC
BC
HC
B
PCA of spiking activity (Hz)
Average topographic position
C
Frequency (Hz)
D
Irregularity (a.u.)
E
Auto-correlation time constant (ms)
F
Entropy (a.u.)
G
Synchrony (a.u.)
H
Dimensionality (a.u.)
I
Cross-correlation space constant (a.u.)
J
Mutual information (a.u.)
GC- GC outdegree
Window of stimulation (ms)